





Article

Photocatalytic Degradation of Neonicotinoid Insecticides over Perlite-Supported TiO₂

Vanja Kosar , Ana-Marija Križanac, Ivana Elizabeta Zelić , Stanislav Kurajica  and Vesna Tomašić 

Faculty of Chemical Engineering and Technology, University of Zagreb, 10000 Zagreb, Croatia; akrizanac@fkit.unizg.hr (A.-M.K.); izelic@fkit.unizg.hr (I.E.Z.); stankok@fkit.unizg.hr (S.K.)

* Correspondence: vkosar@fkit.unizg.hr (V.K.); vtomas@fkit.unizg.hr (V.T.)

Abstract: The aim of this study was to investigate the photocatalytic degradation of the neonicotinoid insecticide acetamiprid in aqueous solution. Experiments were carried out in a 250 mL batch reactor with recirculation of the reaction mixture and using a UVA-LED radiation source with a heterogeneous UVC-modified perlite-based TiO₂ photocatalyst. The photocatalytic degradation of acetamiprid was optimized using a Box–Behnken design (BBD) of the response surface methodology (RSM). The variables in the process optimization were catalyst type, volume of the reaction mixture, and light radiation intensity. From the experimental data obtained, the conversions of the photocatalytic reactions, the reaction rate constants, and the mean square deviations were calculated. The experimental results have shown that the conversion of the reaction is significantly affected by the type of catalyst, i.e., the method used to immobilise the photocatalytic layer on the perlite granules. The highest conversions of 48.49% were reached with catalysts obtained by impregnation methods, while the conversions were quite low (8.68%) for catalysts obtained by sol-gel methods. It was also found that the highest conversions were achieved with the highest radiation intensity and the smallest volume of reaction mixture.

Keywords: acetamiprid; design of experiments (DoE); immobilization; perlite-based TiO₂; photocatalytic degradation; response surface methodology (RSM)



Citation: Kosar, V.; Križanac, A.-M.; Zelić, I.E.; Kurajica, S.; Tomašić, V. Photocatalytic Degradation of Neonicotinoid Insecticides over Perlite-Supported TiO₂. *Processes* **2023**, *11*, 2588. <https://doi.org/10.3390/pr11092588>

Academic Editor: Alina Pyka-Pająk

Received: 19 May 2023

Revised: 27 July 2023

Accepted: 25 August 2023

Published: 29 August 2023



Copyright: © 2023 by the authors. Licensee MDPI, Basel, Switzerland. This article is an open access article distributed under the terms and conditions of the Creative Commons Attribution (CC BY) license (<https://creativecommons.org/licenses/by/4.0/>).

1. Introduction

Insecticides are used primarily to control pests that raid crops or to eliminate insects that transmit diseases in certain areas [1–4]. Neonicotinoid insecticides (NEOs) are the most important and a relatively new class of synthetic insecticides with nicotine-like chemical structures that have been used for insect control in plant and animal protection for several years; they are among the most widely used pesticides [5]. In the last decade, neonicotinoid insecticides have been the fastest growing insecticide class in modern crop protection due to their wide range of applications. They pose relatively low risk to non-target organisms and the environment and have high target specificity compared to other insecticides. However, neonicotinoids have been shown to alter honeybee immunocompetence, and concerns have recently been raised about the adverse effects of imidacloprid on birds [6]. Although some neonicotinoids, such as imidacloprid, thiamethoxam, and clothianidin, have been banned in EU countries for use on agricultural crops attractive to bees since 2013, acetamiprid continues to be approved. However, it was concluded that the potential for high inter-species sensitivity of birds and bees to acetamiprid requires further consideration [7]. Acetamiprid is an organic compound with the chemical formula C₁₀H₁₁ClN₄. The standard name (IUPAC) for acetamiprid is N1-[(6-chloro-3-pyridyl)-methyl]-N2-cyano-N1-methylacetamidine and it belongs to the chloropyridinyl neonicotinoids. It has a very short half-life in the soil and is rapidly degraded by aerobic metabolism. Hydrolytically, it is stable at room temperature and slowly photodegraded in water. Compared to other neonicotinoids, acetamiprid has a lower acute toxicity, and in tests on non-target organisms it was found to

be moderately toxic only to bees [8]. Exposure to acetamiprid occurs primarily through diet (food and water). Professional exposure of individuals who work with this insecticide can occur through dermal contact or inhalation [9].

Heterogeneous photocatalysis is a two- or multiphase system in which reactions occur at the interface between the photocatalyst and the liquid or gaseous phase. During the process, the photocatalyst is in a solid state on a stable substrate [10]. The mechanism of heterogeneous photocatalysis is primarily described by the ability of semiconductors to generate charge carriers upon light irradiation, followed by the formation of free radicals, which leads to further reactions that eventually generate CO_2 and H_2O . Therefore, heterogeneous photocatalysis usually satisfies the following conditions: (i) the pollutants are completely degraded to CO_2 and other inorganic substances, (ii) the process takes place under atmospheric conditions, (iii) the only conditions for the start of the reaction are the presence of oxygen and the energy of UV radiation, both of which can be obtained directly from the air and the sun, (iv) it is possible to deposit the catalyst on various types of inert matrices, including glasses, polymers, carbon nanotubes, and graphene oxides, (v) the catalyst is cheap, nontoxic, and reusable [11]. Heterogeneous photocatalysis has potential applications in the fields of environmental, medical, and civil engineering. The self-cleaning nature of TiO_2 combined with its photocatalytic properties can be used in the production of self-cleaning paints, tiles, surgical equipment, roads, and food preservation. Moreover, heterogeneous photocatalysis is one of the most cost-effective and environmentally friendly methods for water and air purification [11]. To achieve the highest possible efficiency of the photocatalytic process, it is important to choose the appropriate type of photocatalytic reactor. The efficiency of the photoreactor itself is influenced by the mass transfer rate, the reaction rate, and the reaction surface. An ideal photocatalytic reactor would need to have a large specific surface area, a suitable light source that directly irradiates the reaction surface, and a high mass transfer rate, i.e., good mixing/current [12]. The method by which the photocatalytic material is immobilised on the substrate also plays an important role in determining the photocatalytic activity of the photocatalyst. The choice of substrate depends on the type of catalyst used and the pollutant molecule to be degraded. The immobilisation methods must be such that they do not reduce the photocatalytic activity of the photocatalyst. Some of these methods include: the sol-gel method, which consists primarily of dip coating; chemical vapour deposition (CVD), which includes techniques such as atmospheric pressure chemical vapour deposition, plasma-enhanced chemical vapour deposition, organometallic chemical vapour deposition, electrophoretic deposition, and hybrid physical-chemical vapour deposition; heat treatment methods; salt spray methods, etc. [13–17]. Sol-gel and sputtering are popular methods and are used at low temperatures for the immobilisation of photocatalyst nanoparticles on various inert supports [18]. In many cases, it has been observed that the photocatalytic activity of immobilized TiO_2 obtained via the sol-gel method is generally limited by the formation of an amorphous TiO_2 phase after sol-gel synthesis. This can be explained by the fact that photoinduced charge separation is efficient only in crystalline (anatase) phases. To restore this crystalline phase from the amorphous TiO_2 films synthesised by the sol-gel method, thermal treatment at relatively high temperatures is required after deposition, which implies a certain thermal stability [14,19]. Acetamiprid is the subject of numerous studies in the field of heterogeneous photocatalysis, although a search for the keyword “photocatalytic degradation of acetamiprid” in the Google search engine results in four times fewer results than, for example, imidacloprid as a model component [20–26]. However, it is very difficult to compare the results of numerous researchers due to the fact that different photocatalysts that are activated by different radiation sources are usually used, and the studies are also carried out using numerous designs of photoreactors under different operating conditions.

Perlite is a natural volcanic glass that contains 70–75% silicon dioxide (SiO_2) and 2–5% water [27]. In addition to water and SiO_2 , perlite contains 12–15% aluminium oxide (Al_2O_3), 3–4% sodium oxide (Na_2O), 3–5% potassium oxide (K_2O), 0.5–2% iron oxide (Fe_2O_3), 0.2–0.7% magnesium oxide (MgO), and 0.5–1.5% calcium oxide (CaO). The perlite

pieces resemble pearls, hence the name perlite [28]. Water content is a key factor in the specific properties of this mineral. The water bound in the perlite turns into a gas at high temperatures and increases the original volume by 4–20 times, resulting in a lightweight material with high porosity and allowing the perlite to be used in a variety of applications. Perlite is commonly used in soil mixes and as a stand-alone growing medium. It is commonly employed in the building materials industry, where it is used for thermal and acoustic insulation, as aggregate in plaster, mortar, and screed, and for masonry fillings in wall and roof cavities [29]. It is also used in agriculture and horticulture because, when mixed with soil, it has a positive effect on the soil, protecting it from excessive compaction by significantly improving aeration and preventing waterlogging. Perlite has also proved its worth in wastewater treatment, filtration of chemicals, and pharmaceuticals [30,31]. It is the ideal filter medium for large-volume, high-efficiency regenerative filters, swimming pools, and water parks. It is also used as a filter medium in aquarium and pond systems, where it provides biological and mechanical filtration [32].

The design of experiments (DoE) technique [33,34] is very useful for the optimization of photocatalytic processes, since the rate of photocatalytic reaction is influenced by several factors (concentration and type of pollutants, intensity and wavelength of the radiation source, concentration and type of photocatalyst, pH of the solution, temperature, adsorption capacity of the photocatalyst, concentration of the oxidant, etc.) Experiments in which the effects of more than one factor in a reaction are studied are called full-factorial experiments. In a full-factorial experiment, all levels of each factor are compared, and the influence of k variables is monitored, where each variable has a certain number of levels. In a three-level factorial experimental design, the upper and lower levels are labelled +1 and −1, while 0 is the midpoint between the upper and lower levels [35].

The aim of this work is to develop a photocatalytic system for the removal of acetamiprid from simulated leachate and groundwater. For this purpose, a so-called floating photocatalyst based on perlite as an environmentally friendly support is used. The coating of a TiO₂-based photocatalytic layer on the surface of the perlite granules was carried out using three methods. A UVA-LED module is used as a radiation source to simulate sunlight. UV LEDs represent economically efficient energy sources that can be used as backup systems, since they can be used in backup mode during times when there is not enough solar energy available. In addition, the objective of the work is to optimise the above process by applying the design of experiments and response surfaces methodology (DoE & RSM) as an advanced technique that provides insight into the behaviour of the system with the optimal number of experiments performed, thus shortening the path to obtaining useful information about the system under study. We hope that the results obtained will provide guidelines for further work on similar support/photocatalyst systems.

2. Materials and Methods

2.1. Materials and Chemicals

All reagents were of analytical grade and were used without further purification. The analytical standard acetamiprid (PESTANAL™) (purity $\geq 98.0\%$, $\leq 100\%$) used for HPLC analysis was provided by Sigma Aldrich Company Ltd. Laboratory-grade acetamiprid, Boxer Mospilan 200 SP ($w = 20\%$), was provided by Genera Inc., Kalinovica, Croatia. The initial pH values of the reaction mixture were adjusted with sulfuric acid (H₂SO₄) and sodium hydroxide (NaOH) supplied by VWR International S.A.S., Fontenay-sous-Bois, France. The photocatalyst, titanium dioxide (TiO₂-P25) nanopowder containing 80% anatase and 20% rutile with a primary particle size of 30–50 nm and a BET surface area of 50 m²/g, was purchased from Evonik, Essen, Germany. Commercial TiO₂ was modified by UV-C irradiation before photocatalytic measurements. Formic acid 98%, p.a., and HPLC grade acetonitrile were purchased from VWR International, Radnor, PA, USA.

2.2. Photocatalyst Preparation

Heterogeneous catalysts based on perlite on which modified TiO₂ was deposited were prepared using three different methods. The TiO₂ photocatalyst was immobilised on perlite granules in three ways: (a) by the impregnation method without binder, (b) by the impregnation method with the addition of water glass as a binder, and (c) by the sol-gel method. For each method, the same photocatalyst, TiO₂, was used, which was previously pre-treated with UV-C irradiation. A detailed explanation of this pre-treatment procedure that aimed to reduce the band gap energy (E_g) was given elsewhere [36]. The first step was to separate the perlite granules through sieves of different sizes to divide the larger grains from the smaller ones. A sieve with an aperture size of 1.6 mm proved to be optimal. Then, 5 g of the granules with a size of 1.6 mm were weighed, washed in deionized water, and dried.

2.2.1. Immobilisation by Impregnation (Cat-1)

For impregnation with a TiO₂ photocatalyst, 1 g of perlite was weighed. Before application to perlite, 0.5 g of TiO₂ powder (Degussa/Evonik P-25) was added to 18 mL of ethanol to form a dispersion, to which 1.5 mL of dilute nitric acid with a pH of 3.5 was then added to control the pH of the solution. The resulting solution was subjected to ultrasonic sonication (Elmasonic S, without heating) for 5 min to separate the flocculated particles. Then, 1 g of perlite granules was added to the solution and the mixture was sonicated again for 30 min. The wet perlite was then filtered and weighed, followed by calcination at 450 °C for 2 h. The obtained perlite-based catalyst was washed, dried, and weighed before each use. This technique is usually used as a standard method for the preparation of the floating photocatalysts [37].

2.2.2. Immobilisation by Impregnation with Water Glass (Cat-2)

For this procedure, a suspension of 0.5 g TiO₂ powder in 18 mL ethanol and 1.5 mL nitric acid was first prepared. Then, 8 mL of ethanol and 2 mL of water glass (3Na₂O·2SiO₂), which served as a binder, were added. After sonication for 10 min, 1 g of perlite granules was added to the suspension, whereupon the newly formed mixture was sonicated again for 30 min. The wet perlite was then filtered and weighed, followed by calcination at a temperature of 450 °C for 3 h. The obtained perlite-based catalyst was washed, dried, and weighed before each use.

2.2.3. Immobilisation by Sol-Gel Method (Cat-3)

For the sol-gel method, it was necessary to prepare two solutions. In preparing the first solution, 0.36 g of boric acid (H₃BO₃) was first dissolved in 18 mL of titanium (IV) butoxide and 50 mL of ethanol with constant stirring using a magnetic stirrer. Then, 1.5 mL of hydrochloric acid (HCl) was mixed with 10 mL of PEG and the resulting solution was added dropwise to the solution with constant stirring with a magnetic stirrer. This was followed by the addition of perlite and the preparation of a second solution by dissolving 3.6 g of urea in 4.5 mL of deionised water, which was also added to the first solution. It was mixed for 10 min and then sonicated for 1 h until a white gel was formed. The gel obtained was dried at room temperature for 24 h and then in a drying oven for 12 h, forming a xerogel from which the perlite granules were extracted. Then it was calcined at a temperature of 450 °C for 3 h and the obtained granules were weighed. A similar procedure is described in the literature [38].

2.2.4. Characterisation Techniques

The physico-chemical characterisation of the prepared photocatalysts involved nitrogen adsorption–desorption analysis (Brunauer–Emmet–Teller, BET), scanning electron microscopy (SEM) with energy dispersive X-ray (EDX) analysis, and X-ray diffraction (XRD) analysis. The textural properties, such as specific surface areas and average pore diameters, were determined using nitrogen adsorption/desorption at 77 K on a Micrometrics ASAP

2000 apparatus. The surface morphology and EDX analysis of the photocatalytic samples were performed on a Vega 3 Tescan scanning electron microscope. XRD analysis was accomplished using Shimadzu diffractometer XRD 6000 with $\text{CuK}\alpha$ radiation. Data were collected between 10 and 70° (2θ) in a step scan mode, with steps of 0.02° and a counting time of 0.6 s.

2.2.5. Stability and Reusability of the Prepared Floating Photocatalysts

The adherence strength of the TiO_2 -coated perlite particles was investigated with sonication tests. After each sonication, the samples were washed with distilled water and oven-dried at 120°C for 30 min. The adherence strength was then determined based on the percent mass loss of the sample in each test.

To investigate the stability of the prepared floating photocatalysts, the photocatalytic efficiency was evaluated in three cycles to check the reusability of the immobilised photocatalysts. The photocatalyst was washed with double-distilled water and oven-dried at the end of each cycle before the next test.

2.3. Experimental System and Performed Experiments

All experiments were performed in a 250 mL beaker. The beaker is a simple construction of a batch reactor. During the experiment, the reaction mixture circulates continuously in the beaker at a flow rate of 200 mL/min maintained by a peristaltic pump. A UVA-LED module with a power of 30 W and a wavelength of 365 nm was used as the radiation source, which was connected to a voltage source (DC Power Supply, UNI-T UTP3303) and the intensity of the radiation was controlled by the voltage. The UVA-LED module was connected to the Al-heatsink to avoid its overheating. The experimental system is shown in Figure 1. All experiments were carried out with the same initial pH of 6.5 and an initial acetamiprid concentration (C_{ACE}) of 10 ppm, changing the volume of acetamiprid solution, radiation intensity, and catalyst type. A 10 ppm concentration acetamiprid solution was prepared in a 500 mL flask, which required the dissolution of 0.025 g of commercial Mospilane (Genera) [$w(\text{acetamiprid}) = 20\%$] in 500 mL of ultrapure water. Solutions with volumes of 100 , 150 , and 200 mL were placed in a 250 mL beaker. The acetamiprid solution to which the photocatalyst was added was first circulated without a light source (under dark conditions) to ensure the adsorption–desorption equilibrium of acetamiprid on the surface of the photocatalyst before irradiation. After 30 min, a light source (UVA-LED) with radiation intensities of 10 , 20 , and 30 mW/cm^2 was installed, and the photocatalytic reaction started and continued for 4 h. At specific time intervals, 0.5 mL samples were taken from the reactor using a syringe. Before collection into the vials, the collected samples were passed through a 0.22 μm PVDF syringe filter to remove residual suspended photocatalyst particles. The first sample was taken immediately after the addition of the catalyst and the next two samples were taken every 15 min without turning on a light source. Then the UVA-LED was turned on, and the next four samples were taken every 30 min for 2 h, and the last two every hour.

Samples were analysed using a high-performance liquid chromatograph, HPLC (Shimadzu, Kyoto, Japan) equipped with a reversed-phase Agilent Zorbax SB-C18 column (250×4.6 mm, 5 μm) and a UV/VIS detector (SPD-20A). The column temperature was 40°C . The change in acetamiprid concentration in the reaction mixture was monitored over time at a wavelength of 260 nm. Separation was performed in a gradient regime, using 95% water and 5% acetonitrile, with 0.3% formic acid as mobile phase A, 5% water, and 95% acetonitrile, with 0.3% formic acid as mobile phase B at a flow rate of 1 mL min^{-1} .



Figure 1. Experimental system for the photocatalysis process.

3. Results and Discussion

3.1. Characterisation of Photocatalyst

Experiments performed using nitrogen adsorption/desorption at 77 K showed significant differences in the specific surface areas of the investigated samples and small differences in the average pore diameters (Table 1). The specific surface area of the untreated perlite was only $2.09 \text{ m}^2 \text{ g}^{-1}$, with an average pore diameter of 8.42 nm. As expected, immobilisation of TiO_2 on perlite granules leads to a significant decrease in the specific surface areas compared to the parent TiO_2 and to a slight increase in the specific surface areas with respect to the untreated perlite, with a slight deviation of the specific surface area of Cat-2. The average pore diameters of the perlite-supported TiO_2 samples are mainly determined by the characteristic dimensions corresponding to the untreated perlite, regardless of the applied method of immobilisation. The only exception is the Cat-3 sample, with an average pore diameter of 7.56 nm, which is probably due to pore narrowing during the sol-gel method of TiO_2 immobilisation. As will be shown later, the photocatalyst prepared by immobilising TiO_2 on a perlite support using the sol-gel method (Cat-3) showed lower activity compared to the other two immobilisation methods (i.e., Cat-1 and Cat-2).

Table 1. Values of the specific surface areas and average pore diameters.

Sample	Specific Surface Area, $\text{m}^2 \text{ g}^{-1}$	Average Pore Diameter, nm
TiO_2 P25	53.84	9.72
Perlite (untreated)	2.09	8.42
Cat-1	5.56	8.49
Cat-2	1.98	8.39
Cat-3	4.87	7.56

In the XRD diffraction pattern of perlite (Figure 2) only a broad hump roughly between 10 and $40^\circ 2\theta$, typical for amorphous perlite samples, can be observed. In diffraction patterns of titanium-amended perlite samples, this perlite hump is still dominant (Figure 2). However, all three samples also show diffraction maxima of both anatase (ICDD PDF No.21-1272) and rutile (ICDD PDF No.21-1276). Compared to the hump of perlite, the diffraction peaks of anatase and rutile are relatively weak, which indicates a small proportion of titanium in the samples. A comparison of the intensity of the diffraction peak (100) of anatase at 25.28° for all three titanium-amended samples is given as inset in Figure 2. Only in the diffraction pattern of the sample in which titanium was applied to perlite by immersion do the diffraction maxima of titanium phases have slightly greater intensities. The other two samples' diffraction patterns, with titanium immobilised with water glass and sol-gel-derived titanium, show only a traces of anatase and rutile.

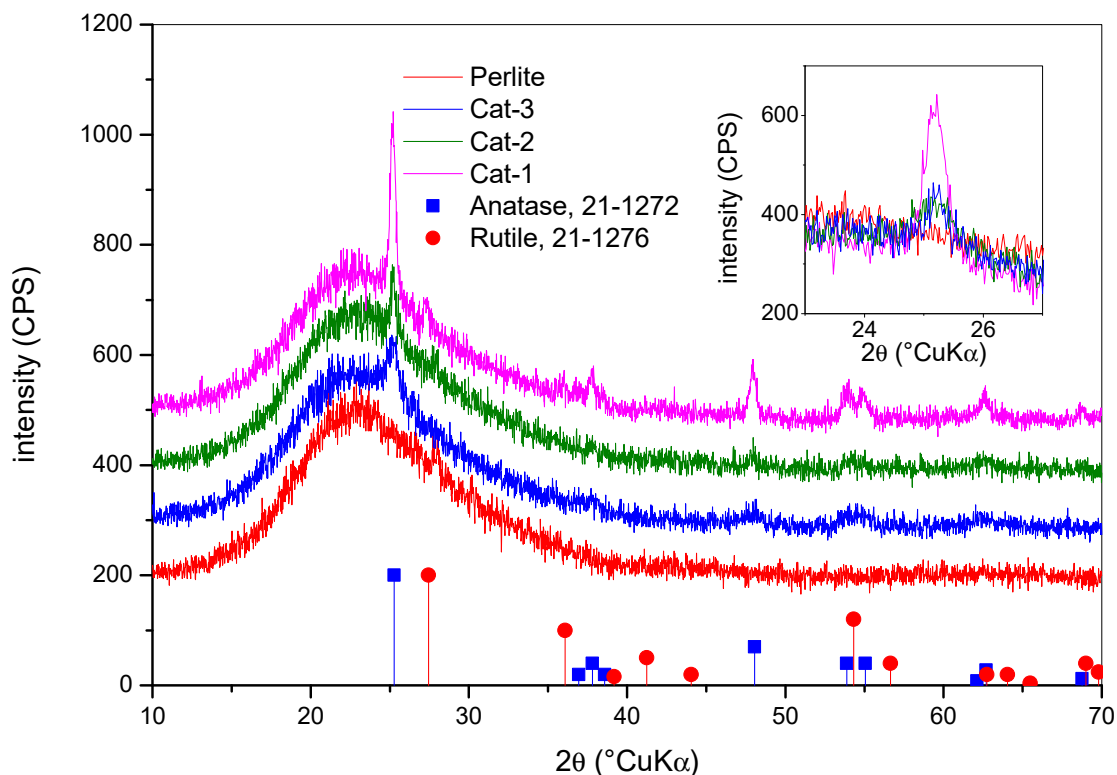


Figure 2. X-ray diffraction patterns of the investigated samples. Patterns are shifted for visualisation purposes. Inset: part of diffraction patterns between 23 and 27° (2θ).

SEM micrographs show the morphologies of the materials studied (Figure 3). As expected, P25 exhibit an agglomerated nanoparticle microstructure (Figure 3a), while expanded perlite shows a typical cellular microstructure (Figure 3b). Such a microstructure enables perlite to be a good carrier for the photocatalytically active titanium dioxide. After TiO_2 deposition, the micrographs clearly show characteristic morphologies of both components (Figure 3c–f). EDS analysis at the spots marked with 1 and 2 in Figure 3d confirmed that the matrix consists mainly of Si and O, while the fine particles are mainly composed of Ti and O. Comparison of the micrographs in Figure 3c,e,f clearly reveals that the deposition of nickel is most successful via the impregnation method, which is in accordance with the results of the XRD analysis.

3.2. Design of Experiments (DoE)

The experiments were designed according to the concept of design of experiments (DoE) with response surface methodology (RSM). This approach is used to determine the functional relationships between the specified process variables (acetamiprid solution volume, source radiation intensity LED, and photocatalyst preparation) and the resulting experimental response (acetamiprid conversion), shown in Table 2. The objective was to determine the key process variables that affect the overall removal process and the optimal values of these variables that maximise the removal efficiency. The identification of relevant process variables is usually done by analysis of variance (ANOVA). The main advantage of DoE is the significant reduction in the number of experiments to be performed, since the behaviour of the interrelated variables can be predicted over a wide range of values. Thus, it is possible to extract the maximum amount of information from a relatively small number of experimental data. The Box–Behnken design (BBD) is a three-step procedure (lowest, average, and highest value of the process variable) within the RSM that is used to optimise experimental conditions and to generate a polynomial regression equation to estimate a response. This technique is generally used when there is a non-linearity between the independent input variables and the dependent response.

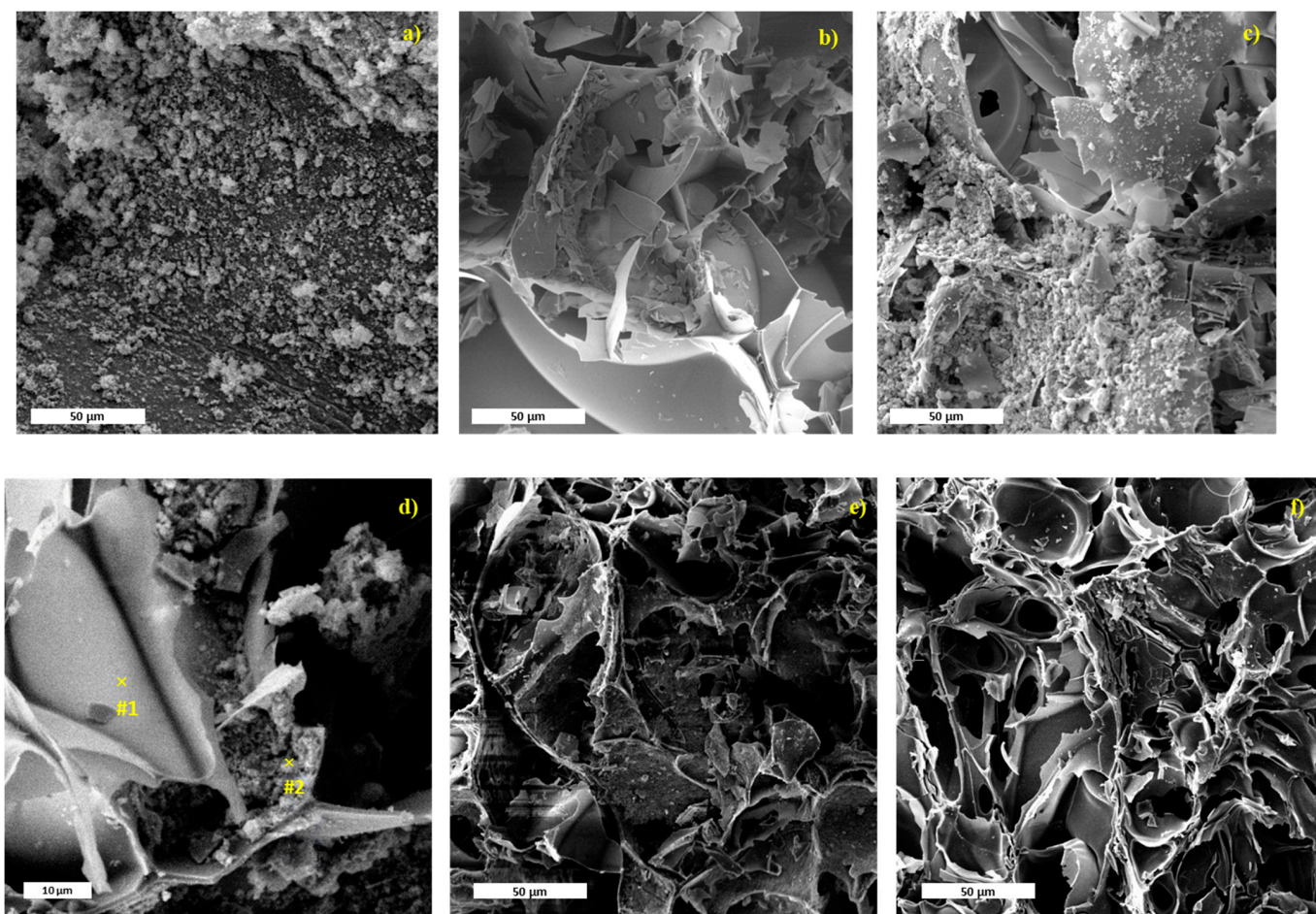


Figure 3. SEM images of: (a) plain TiO_2 , (b) perlite, (c) Cat-1, (d) Cat-1 with marked spots of EDX analysis, (e) Cat-2, and (f) Cat-3.

Table 2. Range of process variables (factors) and their levels.

Factor	Levels		
	Minimum (−1)	Mean (0)	Maximum (1)
A: Volume/mL	100	150	200
B: Radiation Intensity/ mW cm^{-2}	10	20	30
C: Catalyst Preparation/-	Cat-1	Cat-2	Cat-3

3.3. Kinetics of Photocatalytic Acetamiprid Decomposition

The evaluation of reaction kinetics is very important for the assessment and comparison of catalyst performance. Kinetic analysis can also be used to prove the validity of the proposed mechanism, and the term kinetic model usually refers to a mathematical function that describes the dependence of the reaction rate on the variables and parameters of the reaction state. The Langmuir–Hinshelwood (L-H) model is accepted by most researchers, since photocatalytic oxidation occurs on the surface of the photocatalyst [39]. According to the L-H model, the rate of photocatalytic decomposition, r_A , is proportional to the surface coverage of the catalyst by molecules of organic compounds, θ_A :

$$r_A = k\theta_A = \frac{kKc_A}{1 + Kc_A} \quad (1)$$

Since the reaction rate depends on the initial concentration of the reactants, at very low concentrations of the reactant, the denominator in Equation (1) can be neglected, leading to the pseudo-first-order kinetics model (Equation (2)), where k' is the apparent rate constant of the pseudo-first-order reaction ($k' = kK$).

$$r_A = k'c_A \quad (2)$$

Under the experimental conditions used in this study, it is possible to apply a simple model for a batch reactor given by Equation (3).

$$r_A = -\frac{dc_A}{dt} \quad (3)$$

If we associate these two equations with the reaction rate r_A , we get the following.

$$-\frac{dc_A}{dt} = k'c_A \quad (4)$$

The analytical solution of this equation with the initial condition, $t = 0$, $c_A = c_{A0}$, is given by:

$$c_A = c_{A0}e^{-kt} \quad (5)$$

3.4. Influence of Process Variables on Imidacloprid Degradation

The influence of process variables on the degradation of acetamiprid was investigated by performing 13 experiments proposed according to the BBD design. Figure 4 shows the experiments performed, tested with the proposed pseudo-first-order kinetic model. Table 3 shows the estimated values of the parameter k' , as well as the acetamiprid conversions and the root mean square deviations (RMSD), the latter shown in Equation (6).

$$RMSD = \sqrt{\frac{1}{n} \sum_{i=1}^n \left([c_{Ai}/c_{A0}]_{\text{exp}} - [c_{Ai}/c_{A0}]_{\text{mod}} \right)^2} \quad (6)$$

Table 3. Experimental results: total conversion of acetamiprid, estimated rate constants, and RMSD value for each experiment.

Run	Volume, mL	LED Intensity, mW cm ⁻²	Catalyst Preparation	Conversion, %	$k' \times 10^3$, min ⁻¹	RMSD
1	200	20	Cat-1	35.59	1.83	0.051
2	200	20	Cat-3	10.61	0.47	0.012
3	200	30	Cat-2	37.33	1.95	0.028
4	100	10	Cat-2	33.32	1.69	0.015
5	150	30	Cat-3	18.51	0.85	0.019
6	150	20	Cat-2	39.19	2.12	0.018
7	200	10	Cat-2	22.55	1.06	0.039
8	150	30	Cat-1	43.08	2.35	0.024
9	100	20	Cat-1	39.42	2.09	0.022
10	150	10	Cat-1	30.67	1.53	0.035
11	100	20	Cat-3	15.79	0.71	0.013
12	100	30	Cat-2	48.49	2.76	0.038
13	150	10	Cat-3	8.68	0.38	0.008

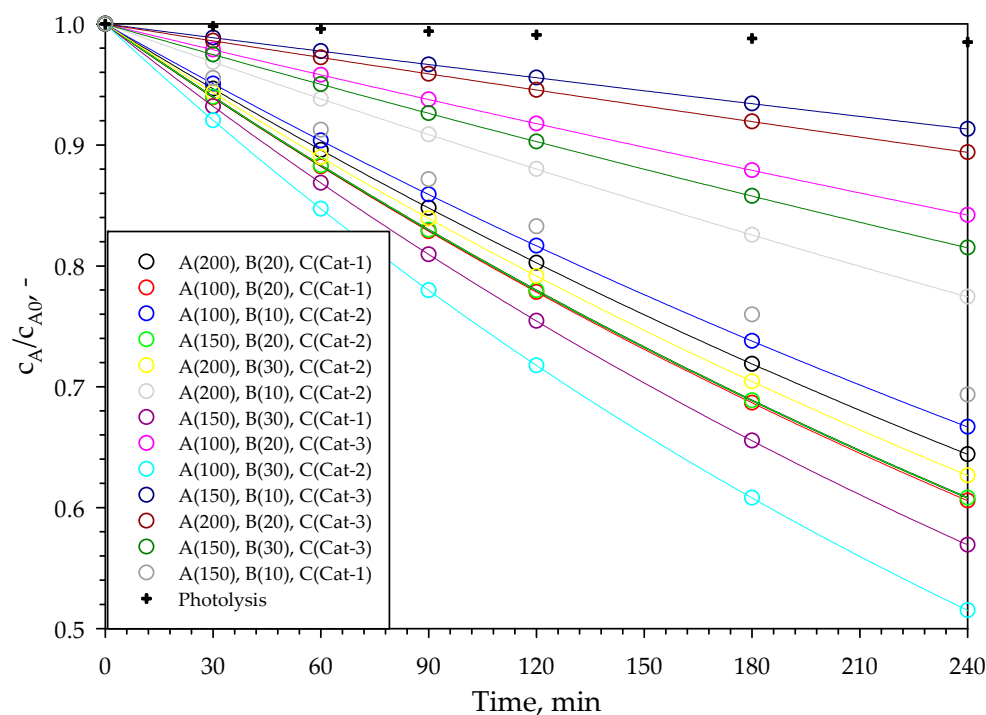


Figure 4. Comparison of the experimental results (points) with the values obtained for the assumed model (lines) under different experimental conditions. Photolysis was performed under the following reaction conditions: initial acetamiprid concentration of 10 ppm, acetamiprid solution volume of 100 mL, recirculation flow rate of 200 mL min⁻¹, radiation intensity of 30 mW cm⁻².

As shown in Table 3, the final conversions after 240 min of photocatalytic degradation of acetamiprid vary from 8.68 to 48.49% depending on the working conditions of the process. The reaction rate constant follows the same trend and varies between 0.38 and $2.76 \times 10^{-3} \text{ min}^{-1}$. In general, based on the low reaction rates, 240 min is not sufficient for complete degradation of acetamiprid under current operating conditions in the batch reactor. The lowest conversion is achieved at the lowest radiation intensity with a photocatalyst (Cat-3) prepared by the sol-gel process. On the contrary, the highest expected conversion is achieved at the highest radiation intensity and the catalyst obtained by impregnation with the addition of water glass as the binder (Cat-2). As expected, significantly higher conversions are obtained in the presence of the floating TiO₂ photocatalyst than in the absence of the photocatalyst (photolysis) (see Figure 4).

3.5. Removal Efficiency Model

The ANOVA analysis proposes a quadratic model to describe the interdependence between the selected dependent variables (solution volume, radiation intensity, and catalyst type as results of the method used to immobilise the photocatalytic layer on the perlite granules) and response (acetamiprid conversion). Given that three dependent variables have been proposed, it would be ideal if the process were described by a cubic model. The reason this is not the case is that the influence of one of the dependent variables is smaller when compared to the other two. In our case, it refers to the volume of acetamiprid solution (factor A). As shown in Table 4, the *p*-value is only slightly less than 0.05 (which means that the factor is significant), but it is significantly higher than the *p*-value for the other two factors (0.0243 and 0.0032, respectively). It appears that the preparation of photocatalysts based on perlite and modified TiO₂ P25 (factor C) under the conditions used in our experimental system had by far the greatest influence on the reaction rate. Surprisingly, the acetamiprid conversions obtained with the sol-gel method, Cat-3, are significantly lower compared to the conversions obtained with the other two preparation methods, Cat-1 and Cat-2 (which are essentially very similar, so the similar conversions

obtained are not surprising). Therefore, in future work, special attention will be paid to the influence of the different parameters of sol-gel synthesis, especially with respect to the detection of Ti ions in the mixture. In our case, obviously, we had much less synthesized TiO_2 compared to that added for suspension processes. Light intensity is also a very important parameter in the photocatalytic process and photoreactor design. Increasing the light intensity leads to more efficient degradation of acetamiprid, which can be attributed to the increased probability of photocatalytic production of reactive radicals. This was confirmed by an experiment [12] carried out with Cat-2 at the highest radiation intensity of 30 mW cm^{-2} and the smallest volume of reaction mixture, 100 mL.

Table 4. Results of ANOVA analysis.

Source	Sum of Squares	df	Mean Square	F-Value	p-Value	
Model	2031.09	9	225.68	15.02	0.0237	Significant
A-Volume	169.37	1	169.37	11.27	0.0438	
B- Radiation Intensity	268.08	1	268.08	17.84	0.0243	
C- Catalyst Preparation	1132.4	1	1132.4	75.36	0.0032	
AB	7.51	1	7.51	0.4996	0.5306	
AC	0.4556	1	0.4556	0.0303	0.8729	
BC	1.68	1	1.68	0.1116	0.7603	
A ²	2.72	1	2.72	0.1807	0.6994	
B ²	3.35	1	3.35	0.2227	0.6692	
C ²	371.43	1	371.43	24.72	0.0156	
Residual	45.08	3	15.03			
Cor Total	2076.17	12				

The Model F-value of 15.02 implies that the model is significant. There is only a 2.37% chance that an F-value this large could occur due to noise. *p*-values less than 0.0500 indicate that model terms are significant. In this case A, B, C, C² are significant model terms. Values greater than 0.1000 indicate that the model terms are not significant.

The theoretical acetamiprid degradation conversions predicted by the Equation (7) are compared with those obtained from the experiments (Figure 5). As can be seen, the proposed model shows good agreement with the experimental results. The coded equation given by Equation (7) is useful for determining the relative influence of the factors by comparing the factor coefficients and can be used to predict the response for a given level of each factor.

$$X_{\text{ACE}} = 39.19 - 3.8675A + 6.5225B - 11.8975C - 0.0975AB - 0.3375AC - 0.6475BC - 1.82375A^2 - 1.94375B^2 - 12.0138C^2 \quad (7)$$

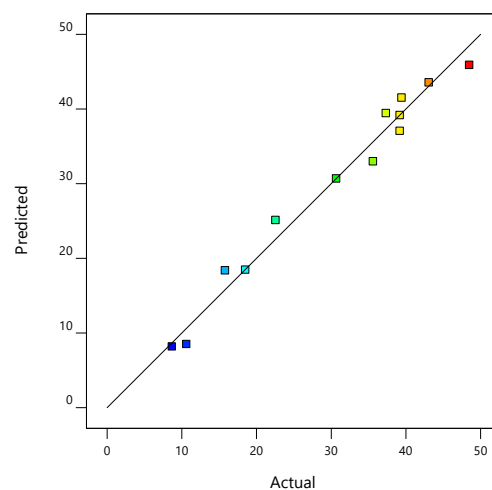


Figure 5. Comparison of the theoretical acetamiprid conversions predicted by the model, Equation (7) (line), and those obtained from the experiments (points).

A graphical interpretation of the model that describes the dependence of acetamiprid conversion on the process variables is shown in Figure 6.

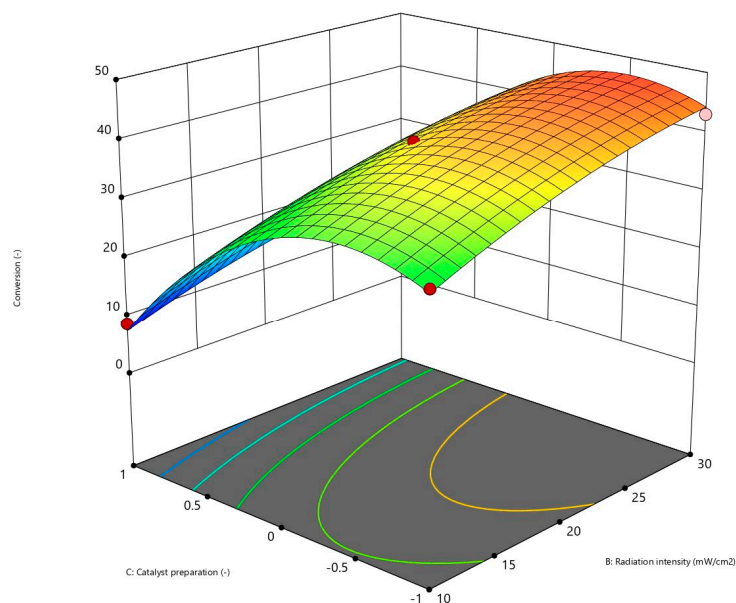


Figure 6. 3D response surfaces for the combined effects of radiation intensity and catalyst preparation on acetamiprid conversion.

3.6. Stability and Reusability of the Perlite-Based TiO₂ Photocatalyst

The stability of the photocatalysts was verified by the adhesion strength of the coated particles, which was investigated with sonication tests. A maximum mass loss of 3% of the samples before and after the sonication test was observed, indicating good stability of the floating photocatalysts, especially in the case of sample Cat-2.

The efficiency of the immobilised perlite-based TiO₂ (Cat-2) for the acetamiprid photodegradation was also examined in three consecutive repeating cycles of the degradation process at the obtained optimum conditions to evaluate its reusability (Figure 7). The degradation efficiencies were comparable, with an insignificant decrease in efficiency after each repeating cycle, which confirms acceptable stability and reusability of the floating perlite-based TiO₂ photocatalyst.

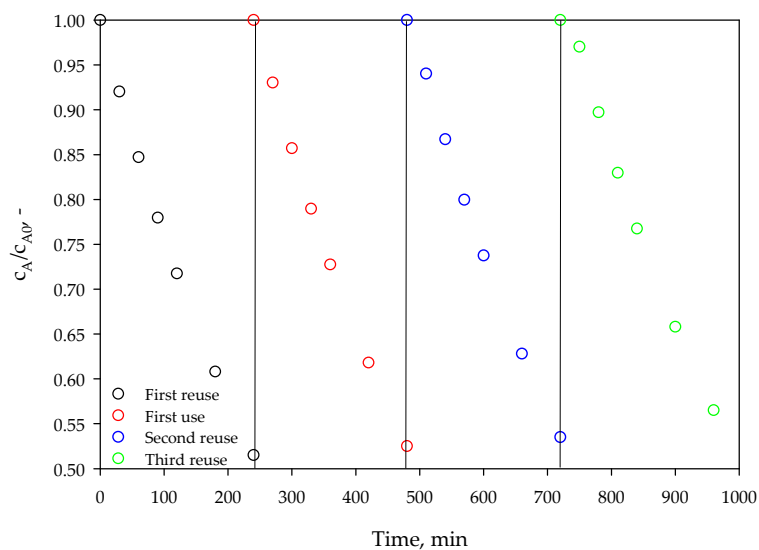


Figure 7. The reusability of the immobilised perlite-based TiO₂ (Cat-2) (reaction conditions: initial acetamiprid concentration of 10 ppm, acetamiprid solution volume of 100 mL, recirculation flow rate of 200 mL min⁻¹, and radiation intensity of 30 mW cm⁻²).

4. Conclusions

In this work, photocatalytic degradation of neonicotinoid acetamiprid was studied in a batch reactor, with recirculation of the reaction mixture using a UVA-LED light source and a modified TiO₂ photocatalyst immobilised on perlite granules using three methods of immobilisation. The XRD, N₂ adsorption/desorption, and SEM analyses were applied for the study of the physicochemical properties of prepared the photocatalysts. The activity of the prepared catalysts was tested, and the effects of the volume of the reaction mixture and the radiation intensity on the degradation efficiency were studied. The experimental data were tested against the kinetic model for the pseudo-first-order reaction. The highest conversions were obtained with the catalysts obtained by impregnation (Cat-1 and Cat-2), while significantly lower conversions were obtained with the catalyst obtained by the sol-gel method (Cat-3). For the same volume of reaction mixture, higher conversion is obtained in the photocatalytic reaction with higher radiation intensity. For the same radiation intensity, a higher conversion is obtained in the photocatalytic reaction with a smaller volume of the reaction mixture. As expected, the highest reaction rate is obtained with the smallest volume (100 mL) and the highest radiation intensity (30 mW cm⁻²). The experimental data show good agreement with a pseudo-first-order kinetic model. Photocatalyst stability and reusability is proven to be rather good after completing several series of consecutive photocatalytic runs. According to our expectations, the easy separation of the floating photocatalysts from treated water systems, good photocatalytic performance, stability, and reusability could contribute to their application in the removal of various pollutants such as pesticides, phenols, antibiotics, and other undesirable compounds, as well as in the remediation and treatment of leachate, oily water, and water from oil spills in the aquatic environment, especially in areas with high exposure and high intensity of natural solar radiation.

Author Contributions: Conceptualisation, V.K. and V.T.; methodology, V.K. and A.-M.K.; investigation, A.-M.K. and I.E.Z.; resources, V.T. and S.K.; data curation, A.-M.K., I.E.Z. and S.K.; writing—original draft preparation, V.K.; writing—review and editing, V.K. and V.T.; visualisation, V.K. and V.T.; supervision, V.K.; funding acquisition, V.T. All authors have read and agreed to the published version of the manuscript.

Funding: The research was funded by Croatian Science Foundation under the projects IN-PhotoCat (IP-2018-01-8669).

Data Availability Statement: The data presented in this study are available upon reasonable request from the corresponding authors.

Conflicts of Interest: The authors declare no conflict of interest.

References

1. Gerot, P. Insecticides: Their route to entry, mechanism of transport and mode of action. *Biol. Rev.* **1983**, *58*, 233–274. [[CrossRef](#)] [[PubMed](#)]
2. Matsumura, F. Classification of insecticides. In *Toxicology of Insecticides*; Springer: New York, NY, USA, 1985; pp. 45–109.
3. Available online: <https://www.epa.gov/caddis-vol2/insecticides> (accessed on 8 May 2023).
4. Available online: <https://www.britannica.com/technology/insecticide> (accessed on 10 May 2023).
5. Anadón, A.; Ares, I.; Martínez, M.; Martínez-Larrañaga, M.-R.; Martínez, M.-A. Neurotoxicity of neonicotinoids. In *Advances in Neurotoxicology*; Aschner, M., Costa, L.G., Eds.; Academic Press: Cambridge, MA, USA, 2020; pp. 167–207.
6. Ensley, S.M. Neonicotinoids. In *Veterinary Toxicology: Basic and Clinical Principles*; Academic Press: Cambridge, MA, USA, 2018; pp. 521–524. ISBN 9780128114100.
7. EFSA Panel on Plant Protection Products and their Residues (PPR); Jerez, A.H.; Adriaanse, P.; Berny, P.; Coja, T.; Duquesne, S.; Focks, A.; Marinovich, M.; Millet, M.; Pelkonen, O.; et al. Statement on the Active Substance Acetamiprid. *EFSA J.* **2022**, *20*, 7031.
8. Wallace, D.R. Acetamiprid. In *Encyclopaedia of Toxicology*, 3rd ed.; 2014; pp. 30–32. Available online: <https://shop.elsevier.com/books/T/A/9780123864550> (accessed on 8 May 2023).
9. La Farré, M.; Pérez, S.; Cantiani, L.; Barceló, D. Fate and toxicity of emerging pollutants, their metabolites and transformation products in the aquatic environment. *Trend. Analyt. Chem.* **2008**, *27*, 991–1007. [[CrossRef](#)]
10. Choi, H.; Al-Abed, S.R.; Dionysiou, D.D.; Stathatos, E.; Lianos, P. TiO₂-based advanced oxidation nanotechnologies for water purification and reuse. In *Sustainability Science and Engineering: Sustainable Water for the Future—Water Recycling versus Desalination*; Escobar, I.I., Schafer, A.I., Eds.; Elsevier Science BV: Amsterdam, The Netherlands, 2010; Chapter 8; Volume 2, pp. 229–254.
11. Ahmed, S.N.; Haider, W. Heterogeneous photocatalysis and its potential applications in water and wastewater treatment: A review. *Nanotechnology* **2018**, *29*, 342001. [[CrossRef](#)]

12. Zhang, Y.; Sillanpää, M. Modification of photocatalyst with enhanced photocatalytic activity for water treatment. In *Advanced Water Treatment: Advanced Oxidation Processes*; Sillanpää, M., Ed.; Elsevier: Amsterdam, The Netherlands, 2020; Chapter 5; pp. 289–366.
13. Ibhaddon, A.; Fitzpatrick, P. Heterogeneous Photocatalysis: Recent Advances and Applications. *Catalysts* **2013**, *3*, 189–218. [[CrossRef](#)]
14. Byrne, C.; Subramanian, G.; Pillai, S.C. Recent advances in photocatalysis for environmental applications. *J. Environ. Chem. Eng.* **2018**, *6*, 3531–3555. [[CrossRef](#)]
15. García-López, E.I.; Marci, G. Preparation of photocatalysts by physical methodologies. In *Materials Science in Photocatalysis*; García-López, E.I., Palmisano, L., Eds.; Elsevier Inc.: Amsterdam, The Netherlands, 2021; Chapter 3; pp. 37–62.
16. Akpan, U.G.; Hameed, B.H. The advancements in sol–gel method of doped-TiO₂ photocatalysts. *Appl. Catal. A Gen.* **2010**, *375*, 1–11. [[CrossRef](#)]
17. Liu, C.; Mao, S.; Shi, M.; Wang, F.; Xia, M.; Chen, Q.; Ju, X. Peroxymonosulfate activation through 2D/2D Z-scheme CoAl-LDH/BiOBr photocatalyst under visible light for ciprofloxacin degradation. *J. Hazard. Mater.* **2021**, *420*, 126613. [[CrossRef](#)] [[PubMed](#)]
18. Singh, S.; Mahalingam, H.; Singh, P.K. Polymer-supported titanium dioxide photocatalysts for environmental remediation: A review. *Appl. Catal. A Gen.* **2013**, *462*, 178–195. [[CrossRef](#)]
19. Cunha, L.D.; Kuznetsov, A.; Achete, C.A.; da Hora Machado, A.E.; Marques, M. Immobilised TiO₂ on glass spheres applied to heterogeneous photocatalysis: Photoactivity, leaching and regeneration. *PeerJ* **2018**, *6*, e4464. [[CrossRef](#)] [[PubMed](#)]
20. Guzsavány, V.J.; Csanádi, J.J.; Lazić, S.D.; Gaál, F.F. Photocatalytic degradation of the insecticide acetamiprid on TiO₂ catalyst. *J. Braz. Chem. Soc.* **2009**, *20*, 152–159. [[CrossRef](#)]
21. Banić, N.D.; Šojić, D.V.; Krstić, J.B.; Abramović, B.F. Photodegradation of neonicotinoid active ingredients and their commercial formulations in water by different advanced oxidation processes. *Water Air Soil Pollut.* **2014**, *225*, 1954. [[CrossRef](#)]
22. Fenoll, J.; Garrido, I.; Hellín, P.; Flores, P.; Navarro, S. Photodegradation of neonicotinoid insecticides in water by semiconductor oxides. *Environ. Sci. Pollut. Res.* **2015**, *22*, 15055–15066. [[CrossRef](#)] [[PubMed](#)]
23. Acero, J.L.; Real, F.J.; Benitez, F.J.; Matamoros, E. Degradation of neonicotinoids by UV irradiation: Kinetics and effect of real water constituents. *Sep. Purif. Technol.* **2019**, *211*, 218–226. [[CrossRef](#)]
24. González, T.; Dominguez, J.R.; Correia, S. Neonicotinoids removal by associated binary, tertiary and quaternary advanced oxidation processes: Synergistic effects, kinetics and mineralization. *J. Environ. Manag.* **2020**, *261*, 110156. [[CrossRef](#)] [[PubMed](#)]
25. Lee, Y.-J.; Kang, J.-K.; Park, S.J.; Lee, C.-G.; Moon, J.K.; Alvarez, P.J.J. Photocatalytic degradation of neonicotinoid insecticides using sulfate-doped Ag₃PO₄ with enhanced visible light activity. *Chem. Eng. J.* **2020**, *402*, 126183. [[CrossRef](#)]
26. Sayury Miyashiro, C.; Hamoudi, S. Aqueous acetamiprid degradation using combined ultrasonication and photocatalysis under visible light. *Water Air Soil Pollut.* **2022**, *233*, 401. [[CrossRef](#)]
27. Available online: <http://amit-online.de/en/perlite-expansion-plants/basic-characteristics-and-application-areas-of-perlite/> (accessed on 10 May 2023).
28. Samar, M.; Saxena, S. Study of chemical and physical properties of perlite and its application in India. *Int. J. Sci. Technol. Manag.* **2016**, *5*, 70–79.
29. Papadopoulos, A.P.; Bar-Tal, A.; Silber, A.; Saha, U.K.; Raviv, M. Inorganic and synthetic organic components of soilless culture and potting mixes. In *Soilless Culture: Theory and Practice*; Raviv, M., Lieth, J.L., Eds.; Academic Press: San Diego, CA, USA; Elsevier BV: Amsterdam, The Netherlands, 2008; Chapter 12; pp. 505–544.
30. Maxineasa, S.G.; Isopescu, D.N.; Lupu, M.L.; Baci, I.-R.; Pruna, L.; Somacescu, C. The use of perlite in civil engineering applications. *IOP Conf. Ser. Mater. Sci. Eng.* **2022**, *1242*, 012022. [[CrossRef](#)]
31. Available online: <https://www.perlite.org/wp-content/uploads/2018/03/perlite-for-filtration.pdf> (accessed on 10 May 2023).
32. Maxim, L.D.; Niebo, R.; McConnell, E.E. Perlite toxicology and epidemiology—A review. *Inhal. Toxicol.* **2014**, *26*, 259–270. [[CrossRef](#)]
33. Montgomery, D.C. *Design and Analysis of Experiments*, 6th ed.; John Wiley & Sons Inc.: Hoboken, NJ, USA, 2005.
34. Myers, R.H.; Montgomery, D.C.; Anderson-Cook, C.M. *Response Surface Methodology: Process and Product Optimisation Using Designed Experiments*, 3rd ed.; John Wiley & Sons Inc.: Hoboken, NJ, USA, 2016.
35. Barka, N.; Abdennouri, M.; Boussaoud, A.; Galadi, A.; Baâlala, M.; Bensitel, M.; Sahibed-Dine, A.; Nohair, K.; Sadiq, M. Full factorial experimental design applied to oxalic acid photocatalytic degradation in TiO₂ aqueous suspension. *Arab. J. Chem.* **2014**, *7*, 752–757. [[CrossRef](#)]
36. Babić, K.; Tomašić, V.; Gilja, V.; Le Cunff, J.; Gomzi, V.; Pintar, A.; Žerjav, G.; Kurajica, S.; Duplančić, M.; Zelić, I.E.; et al. Photocatalytic degradation of imidacloprid in the flat-plate photoreactor under UVA and simulated solar irradiance conditions—The influence of operating conditions, kinetics and degradation pathway. *J. Environ. Chem. Eng.* **2021**, *9*, 105611. [[CrossRef](#)]
37. Hosseini, S.N.; Borghei, S.M.; Vossoughi, M.; Taghavinia, N. Immobilization of TiO₂ on perlite granules for photocatalytic degradation of phenol. *Appl. Catal.* **2007**, *74*, 53–62. [[CrossRef](#)]

38. Wang, X.; Wang, W.; Zhang, J.; Zhao, J.; Gu, Z.; Zhou, L. Synthesis, structural characterization and evaluation of floating B-N codoped TiO₂/expanded perlite composites with enhanced visible light photoactivity. *Appl. Surf. Sci.* **2015**, *349*, 264–271. [[CrossRef](#)]
39. Olis, D.F. Kinetics of photocatalyzed reactions: Five lessons learned. *Front. Chem.* **2018**, *6*, 378. [[CrossRef](#)] [[PubMed](#)]

Disclaimer/Publisher's Note: The statements, opinions and data contained in all publications are solely those of the individual author(s) and contributor(s) and not of MDPI and/or the editor(s). MDPI and/or the editor(s) disclaim responsibility for any injury to people or property resulting from any ideas, methods, instructions or products referred to in the content.